NASA/TM—2005-213564 AIAA–2005–0514

Experimental Investigation of the Differences Between Reynolds-Averaged and Favre-Averaged Velocity in Supersonic Jets

J. Panda
Ohio Aerospace Institute, Brook Park, Ohio

R.G. Seasholtz
Glenn Research Center, Cleveland, Ohio

May 2005

The NASA STI Program Office . . . in Profile

Since its founding, NASA has been dedicated to the advancement of aeronautics and space science. The NASA Scientific and Technical Information (STI) Program Office plays a key part in helping NASA maintain this important role.

The NASA STI Program Office is operated by Langley Research Center, the Lead Center for NASA's scientific and technical information. The NASA STI Program Office provides access to the NASA STI Database, the largest collection of aeronautical and space science STI in the world. The Program Office is also NASA's institutional mechanism for disseminating the results of its research and development activities. These results are published by NASA in the NASA STI Report Series, which includes the following report types:

- TECHNICAL PUBLICATION. Reports of completed research or a major significant phase of research that present the results of NASA programs and include extensive data or theoretical analysis. Includes compilations of significant scientific and technical data and information deemed to be of continuing reference value. NASA's counterpart of peer-reviewed formal professional papers but has less stringent limitations on manuscript length and extent of graphic presentations.

- TECHNICAL MEMORANDUM. Scientific and technical findings that are preliminary or of specialized interest, e.g., quick release reports, working papers, and bibliographies that contain minimal annotation. Does not contain extensive analysis.

- CONTRACTOR REPORT. Scientific and technical findings by NASA-sponsored contractors and grantees.

- CONFERENCE PUBLICATION. Collected papers from scientific and technical conferences, symposia, seminars, or other meetings sponsored or cosponsored by NASA.

- SPECIAL PUBLICATION. Scientific, technical, or historical information from NASA programs, projects, and missions, often concerned with subjects having substantial public interest.

- TECHNICAL TRANSLATION. English-language translations of foreign scientific and technical material pertinent to NASA's mission.

Specialized services that complement the STI Program Office's diverse offerings include creating custom thesauri, building customized databases, organizing and publishing research results . . . even providing videos.

For more information about the NASA STI Program Office, see the following:

- Access the NASA STI Program Home Page at ***http://www.sti.nasa.gov***

- E-mail your question via the Internet to help@sti.nasa.gov

- Fax your question to the NASA Access Help Desk at 301–621–0134

- Telephone the NASA Access Help Desk at 301–621–0390

- Write to:
  NASA Access Help Desk
  NASA Center for AeroSpace Information
  7121 Standard Drive
  Hanover, MD 21076

NASA/TM—2005-213564 AIAA–2005–0514

Experimental Investigation of the Differences between Reynolds-Averaged and Favre-Averaged Velocity in Supersonic Jets

J. Panda
Ohio Aerospace Institute, Brook Park, Ohio

R.G. Seasholtz
Glenn Research Center, Cleveland, Ohio

Prepared for the
43rd Aerospace Sciences Meeting and Exhibit
sponsored by the American Institute of Aeronautics and Astronautics
Reno, Nevada, January 10–13, 2005

National Aeronautics and
Space Administration

Glenn Research Center

May 2005

Acknowledgments

We acquired these experimental data as part of a jet noise source identification study. J. Panda acknowledges encouragements from Dr. James Bridges of NASA Glenn Research Center in performing this part of data analysis. The work was funded by NASA's Quiet Aircraft Technology program.

Available from

NASA Center for Aerospace Information
7121 Standard Drive
Hanover, MD 21076

National Technical Information Service
5285 Port Royal Road
Springfield, VA 22100

Available electronically at http://gltrs.grc.nasa.gov

Experimental Investigation of the Differences Between Reynolds-Averaged and Favre-Averaged Velocity in Supersonic Jets

J. Panda
Ohio Aerospace Institute
Brook Park, Ohio 44142

R.G. Seasholtz
National Aeronautics and Space Administration
Glenn Research Center
Cleveland, Ohio 44135

Abstract

Recent advancement in the molecular Rayleigh scattering based technique allowed for simultaneous measurement of velocity and density fluctuations with high sampling rates. The technique was used to investigate unheated high subsonic and supersonic fully expanded free jets in the Mach number range of 0.8 to 1.8. The difference between the Favre averaged and Reynolds averaged axial velocity and axial component of the turbulent kinetic energy is found to be small. Estimates based on the Morkovin's 'Strong Reynolds Analogy' were found to provide lower values of turbulent density fluctuations than the measured data.

I. Introduction

Reynolds averaging involves dividing a fluid flow parameter w into a time-averaged $\overline{w}$, and a fluctuating w' part:

$$w(t) = \overline{w} + w'(t), \quad \overline{w} = \lim_{T\to\infty} \frac{1}{T}\int_0^T w\, dt \tag{1}$$

In the Favre-averaging process a density-weighted filtering is used to calculate time average $\widetilde{w}$ and the remaining fluctuating part w'':

$$w(t) = \widetilde{w} + w''(t), \quad \widetilde{w} = \frac{1}{\overline{\rho}} \lim_{T\to\infty} \frac{1}{T}\int_0^T \rho\, w\, dt \tag{2}$$

where ρ denotes air density. As there is no mass flux across the Favre-averaged streamline, the use of the Favre-averaged variables makes the governing equations for the mean density, mean velocity and the mean enthalpy more compact. In compressible flow, such simplifications are unattainable by the Reynolds averaging process. Experimental data, such as those measured by Particle image Velocimetry and the present Rayleigh scattering technique, however, produce Reynolds averaged quantities. The differences between the two averages for parameters such as the axial velocity u and the turbulent kinetic energy become a concern whenever computational results are to be compared against experimental data.

The present effort is to determine the differences experimentally by measuring correlations between density and axial velocity fluctuations.

The measurements have been possible due to the recent advances in a molecular Rayleigh scattering based technique to simultaneously measure density and velocity fluctuations in high-speed flows (Seasholtz, Panda, and Elam, 2002). Fluctuations occurring over a frequency range of 0 to 50 kHz have been measured. The technique is based on laser light scattering from the gas molecules present in air. Since neither any seed particles nor any intrusive probes are used, the technique is strictly non-invasive. Implementation of the technique requires special attention to the cleanliness of the air stream, isolation of the sensitive optical components from jet noise, usage of a Fabry-Perot interferometer and low-level light measuring electronics. Description of the technique is provided later in the text.

The present work is part of a database development project and the free jets used for the current investigation were also the subject of some of the earlier studies. The time averaged velocity $\overline{u}$, temperature $\overline{T}$, and density $\overline{\rho}$ surveys from these jets have been reported by Panda, Seasholtz, Elam, and Mielke (2004). Schlieren photographs and various statistics of density fluctuations were provided in Panda and Seasholtz (2002). The far field noise sources were identified by correlating turbulent density and velocity fluctuations with far field noise pressure fluctuations in Panda, Seasholtz, and Elam (2003) and Panda and Seasholtz (2002).

A second goal of the present work is to validate Morkovin's strong Reynolds analogy in unheated jets. The origin of Favre averaging to remove density fluctuations from the time-averaged equations of motion lies with this hypothesis. A physically intuitive description of the hypothesis can be found in a review article by Peter Bradshaw (1977*): "It is generally accepted that the direct effects of density fluctuations on turbulence are small if the root-mean-square density fluctuation is small compared with the absolute density: this is Morkovin's hypothesis . . . This means that the turbulence structure of boundary layers and wakes at free-stream Mach numbers . . . less than about 5, and of jets at Mach numbers less than about 1.5, is closely the same as in the corresponding constant-density flow.*"

"In compressible turbulent flows the velocity, temperature and density… all fluctuate; in analytical work it is more convenient . . . to treat the equivalent fluctuations of vorticity, entropy (or total temperature), and acoustic pressure. Morkovin's important contribution . . . was to use the limited data available in 1961 to show that in non-hypersonic boundary layers the acoustic mode is negligible…and the entropy (total temperature) mode is very small for conventional rates of heat transfer . . . It follows from Morkovin's findings that

$$\frac{p'}{\overline{p}} << 1, \quad \frac{T_0{}'}{T_0} << 1$$
$$\text{so that } \frac{\rho'}{\overline{\rho}} \approx -\frac{T'}{\overline{T}} \approx (\gamma - 1)M^2 \frac{u'}{\overline{u}}. \tag{3}$$

The direct quote ends at the equation. In the above, p is static pressure, T_0 is total temperature, ρ is gas density, T is static temperature, γ is the ratio of specific heats, u is the axial component of velocity and M is the local Mach number based on the local velocity and the local speed of sound.

Validation of the Morkovin's hypothesis and measurements of the Favre averaged variables has been attempted in the past using hot-wire anemometry. The signal analysis from hot-wires becomes involved and carries various assumptions for applications in compressible flows. The advancement of the optical measurement techniques brought new tools better suited for the high velocity flows. Bowersox (1996) used Laser Doppler Anemometry in conjunction with hot-wires to provide a more straight forward measurement of Favre averaged velocity and Reynolds stresses. These efforts were mostly confined to the wall-bounded shear layers. In free shear layer hot-wires break easily and the authors do not know of any earlier study addressing the present goals.

Difference Between Favre-Averaged and Reynolds-Averaged Axial Velocity and Axial Component of Kinetic Energy

Following the definitions of Reynolds averaging and Favre averaging shown in equations (1) and (2)

$$\tilde{u} = \frac{\overline{\rho u}}{\overline{\rho}} = \frac{\overline{(\rho' + \overline{\rho})(u' + \overline{u})}}{\overline{\rho}} = \overline{u} + \frac{\overline{\rho' u'}}{\overline{\rho}} \tag{4}$$

$$\text{Hence, } \tilde{u} - \overline{u} = \frac{\overline{\rho' u'}}{\overline{\rho}} \tag{5}$$

Therefore, the differences in the time averaged velocity is due to the correlations between the density and velocity fluctuations. A similar equation holds for the fluctuating terms. Since $\tilde{u} + u'' = \overline{u} + u'$,

$$u' - u'' = \frac{\overline{\rho' u'}}{\overline{\rho}} \tag{6}$$

Next kinetic energy is considered which involves product of fluctuations. For example Reynolds-averaged kinetic energy $k = 0.5\left(\overline{u'u'} + \overline{v'v'} + \overline{w'w'}\right)$, where v and w represent respectively, radial and tangential components of velocity. In the present program only the axial component of velocity was measured. The axial component of kinetic energy in Favre-averaged fluctuations:

$$\widetilde{u''u''} = \frac{\overline{\rho u''u''}}{\overline{\rho}} = \frac{\overline{(\overline{\rho} + \rho')u''u''}}{\overline{\rho}} = \overline{u''u''} + \frac{\overline{\rho' u''u''}}{\overline{\rho}} \tag{7}$$

Using equation (6) the first term on the right hand side can be expressed as:

$$\overline{u''u''} = \overline{u'u'} + \left(\frac{\overline{\rho' u'}}{\overline{\rho}}\right)^2 \tag{8}$$

The second term on the right hand side of equation (7) can also be written as:

$$\frac{\overline{\rho' u''u''}}{\overline{\rho}} = \frac{\overline{\rho' u'u'}}{\overline{\rho}} - 2\left(\frac{\overline{\rho' u'}}{\overline{\rho}}\right)^2 \tag{9}$$

Hence, the difference in axial component of kinetic energy:

$$\frac{1}{2}\left(\widetilde{u''u''} - \overline{u'u'}\right) = \frac{1}{2}\left(\frac{\overline{\rho' u'u'}}{\overline{\rho}} - \left(\frac{\overline{\rho' u'}}{\overline{\rho}}\right)^2\right) \tag{10}$$

Above equation shows that in addition to density-velocity correlations, density-velocity^2 correlations have significant contributions to the difference. In the present work these two correlations were calculated from cross-correlations defined as:

$$\langle \rho' ; u' \rangle(\tau) = \frac{1}{T}\int_0^T \rho'(t)\, u'(t+\tau)\, dt$$
$$\text{and, } \langle \rho' ; u'u' \rangle(\tau) = \frac{1}{T}\int_0^T \rho'(t)\, [u'(t+\tau)]^2\, dt \tag{11}$$

where τ is the correlation time or delay time and T is the duration of the measured data. Note that by definition:

$$\overline{\rho' u'} = \langle \rho' ; u' \rangle_{\tau=0} \text{ and, } \overline{\rho' u' u'} = \langle \rho' ; u' u' \rangle_{\tau=0} \tag{12}$$

Fundamentals of Flow Measurement Using Rayleigh Scattering Principle

A simplistic description of the measurement process, using laser induced Rayleigh scattering is schematically shown in figure 1. When a laser beam is allowed to pass through a gas, the molecules present in the gas cause light scattering. The Rayleigh scattering process describes most (~99 percent) of the molecular scattered light. In the present experiment scattered light is collected and spectrally resolved to measure velocity. The line width of the incident laser beam is very narrow while that of the Rayleigh scattered light is wide. Even if the gas medium is stationary, the random thermal motion of the gas molecules creates a wide range of Doppler shift—resulting in a spectral broadening of the collected light. The Full Width at Half Maximum (FWHM) is a function of the distribution of molecular velocities and, therefore, is a measure of gas temperature. In the case of a moving gas media, the bulk velocity is superimposed on the random thermal motion of the individual molecules; therefore separation between the peaks of the incident laser line and the Rayleigh spectrum provides a measure of the bulk velocity. The total light under the Rayleigh spectrum is proportional to the molecular number density and provides a measure of gas density. Thus a single Rayleigh spectrum carries information of one component of gas bulk velocity, temperature and density.

This basic principle has been used in the past to measure *time-averaged* quantities. Since density variation modulates the total scattered light, unsteady density fluctuations are easier to measure. Extension of the Rayleigh scattering technique to measure *unsteady* velocity fluctuation has remained a challenge. Recently, Seasholtz, Panda, and Elam (2002) have simultaneously measured the time variation of density and velocity fluctuations in free jets. The present setup is for a point-measuring system; a continuous wave laser was used, and scattered light from a small region was spectrally analyzed using a Fabry-Perot interferometer.

To illustrate the unsteady velocity measurement process, first the nature of a fringe formed by the interferometer is shown in figure 2. The interferometer basically images the fiber-end delivering the scattered light. Since the fiber diameter is small, the field of view in the image covers a fraction of the free spectral range. The spectral analysis is a two-step process. First, a small portion of the light directly out of the laser beam is imaged through the interferometer (the Rayleigh scattered light is blocked; instead a part of the unscattered incident laser beam is analyzed). The narrow line width of the laser makes a sharp, narrow ring in this image (reference image, fig. 2(a)). In the second step the Rayleigh scattered light from a moving gas medium is passed through the fiber. The image formed by the Fabry-Perot interferometer (Rayleigh image, fig. 2(b)) is different: a diffused ring with a different ring diameter results. The radial shift in the peak intensity locations between the Rayleigh and the reference images is related to the Doppler shift associated with the bulk motion of the air stream (the diffused nature of the Rayleigh image is due to the thermal broadening). Since the laser frequency, and therefore, the reference fringe are fixed, an instantaneous change of air velocity produces a radial shift of the ring seen in the

Rayleigh image. To measure the time variation of velocity one needs to monitor the ring diameter in the Rayleigh image. To this end Seasholtz et al. (2002) used an image dissector that split the Rayleigh image into two concentric parts (fig. 2(c)), and measured the ratio of light intensities from the inner and the outer parts using two photomultiplier tubes (PMT). The ratio of photoelectron counts from the two PMT carried information about the ring diameter variation in the Rayleigh image, which in turn reflected the change of Doppler shift frequency from velocity change at the probe volume. For calibration, the intensity variations from the two parts were measured from known velocity flows. It was found that the intensity variations in either part of the image can be modeled by second order polynomials. If N_2 and N_3 denote photo-electron count rates from the inner and outer PMTs then:

$$\begin{aligned} N_2 &= A_i + uB_i + u^2 C_i \,, \\ N_3 &= A_o + u B_o + u^2 C_o \end{aligned} \tag{13}$$

Where, A_i, B_i, C_i, A_o, B_o and C_o are calibration constants. The velocity component u is measured from a ratio of the two counts, $R=N_3/N_2$:

$$u = \frac{-(RB_i - B_o) + \sqrt{(RB_i - B_o)^2 - 4(RA_i - A_o)(RC_i - C_o)}}{2(RC_i - C_o)} \tag{14}$$

Note that the ratio of two counts cancels out changes in overall scattering intensity associated with flow density variation. Also the physically meaningful, positive root of the quadratic equation is considered. The component of velocity measured using a given optical arrangement depends on the angular position of the collection lens with respect to the incident laser beam. The present setup, shown in figure 3, measured the axial velocity component. Note that the setup measures negative –u velocity. The calibration process accounted for the sign reversal. The Rayleigh scattered light was collected and transmitted to an adjoining room for spectral analysis. Figure 4 shows a schematic of the spectroscopic arrangement.

An important caveat in the above analysis is an implicit assumption that the effect of temperature fluctuations is also accounted for via the calibration process. Temperature broadening results in changes of light intensity in both the inner and outer parts of the image. By virtue of measuring a ratio of intensities between the two parts of the image, the process was made somewhat insensitive to temperature fluctuations. A numerical uncertainty analysis (Seasholtz et al. 2001) demonstrates that the effect of temperature fluctuation is small compared to the bigger change associated with velocity fluctuations. In addition, the present experiment was conducted in the potential core of the same free jets used to obtain calibration constants. Hence, the influence of isentropic temperature fluctuations was automatically included in the calibration constant. However, non-isentropic temperature fluctuations have affected the velocity fluctuations data in a small yet unknown way.

To measure density fluctuations about 10 percent of the Rayleigh scattered light was split off using a beam splitter (BS1 in fig. 4) and the intensity fluctuations were monitored using a separate photo-multiplier tube. For a fixed optical setup and a fixed gas composition, the intensity variation of Rayleigh scattered light is directly proportional to air density variation. Once again, a calibration is necessary to relate photo-electron count to density change. The calibration was performed in the same core regions of the jet flows used for velocity calibration. If the local air density is ρ and photo-electron count rate from PMT1 is N_1 then:

$$N_1 = C_{\rho 1} + \rho C_{\rho 2} \,. \tag{15}$$

Where, $C_{\rho 1}$ and $C_{\rho 2}$ are calibration constants. In summary, a total of three PMTs were: two for measuring velocity and one for density. Additionally two sets of calibration constants were needed for velocity and density measurements.

II. Experimental Set-Up

Experiments were performed at NASA Glenn Research Center using three different nozzles (one convergent and two convergent-divergent) operated at Mach numbers, M = 0.95, 1.4 and 1.8. The convergent-divergent nozzles were designed by the method of characteristics. All nozzles were 25.4 mm in exit diameter. The jet facility used a continuous supply of unheated compressed air. The Rayleigh scattering system is somewhat elaborate and the following provides a brief description of some of the central features. An in-depth discussion of the Rayleigh set-up can be found in Seasholtz, Panda, and Elam (2002). The optical system was built in two parts. The first one is around the jet facility for transmitting laser light and collecting the scattered light (fig. 3). The scattered light was then passed through a 0.55 mm diameter optical fiber to a quiet room where the second part, consisting of a spectroscopic system and photon counting electronics, were placed (fig. 4). The splitting of the setup is necessary to minimize the effect of vibration on the optical components. Additional care had to be taken to reduce dust particles in air streams, and to stabilize the interferometer from temperature and vibration induced drifts. To reduce dust particles the dry air, supplied from a central high-pressure facility, was passed through additional micron size filters which made the primary jet air very clean. To clean the entrained ambient air, an additional air blower and filter system was installed that provided a large, 200 mm diameter, low-speed (~20 m/s) co-flow around the 25.4 mm primary jet.

The optical system was built over an X-Y traversing unit that carried laser head, transmission and collection optics. Surveys were made by moving the probe volume from point to point in the plume. The laser head of the solid-state, frequency-doubled, Nd:VO_4 laser was placed at the bottom part of the set-up. About 5 watts of single mode, 532 nm wavelength laser light was transmitted through a hollow side beam that contained a half-wave plate, focusing lens, mirrors and baffles. Since Rayleigh scattered light is polarization dependent, the half-wave plate was rotated to align the peak scattering plane with receiving optics. The background scattered laser light was significantly attenuated by suitable use of baffles and beam-dump. It was found that the noise from the jet created a tonal excitement of the laser line at around 430 Hz. To reduce this excitation, an anechoic box was built around the laser head. This box significantly reduced the laser unsteadiness, but a trace remained and was manifested in the experimental results.

To measure axial component of velocity the laser beam was passed at 45° to the jet axis, and scattered light from 90° to the incident direction was collected by lenses placed in the same plane containing the laser beam and the jet axis. The collection optics was made of a collimator (300 mm focal length, 82 mm diameter achromat) and a focusing lens (160 mm focal length achromat) that imaged the probe volume on the face of a 0.55 mm diameter multimode fiber. The combination of the fiber diameter and the magnification ratio of the collection optics defined the probe volume length to 1.03 mm. Not shown in figure 3 is an additional part of the set-up where a small part of light from the transmitting laser beam was split off for the purpose of monitoring laser frequency as well as to maintain the alignment in Fabry-Perot interferometer. Whenever necessary, a pneumatically actuated mirror was placed in the transmission laser path to divert light towards a diffuser. The mirror also blocked the incident laser beam from going through the jet, and the diffuser scattered the incident light; a small part of which was then collected by the optical fiber.

In the second part of the setup (fig. 4) light arriving via the optical fiber was collimated by 100 mm focal length lens L1, and about 10 percent was split by BS1 and measured by PMT1. Output from PMT1 was proportional to the air density fluctuations. The rest of the collimated beam was passed through a 70 mm aperture planer mirror Fabry-Perot interferometer for spectral analysis. Single wavelength light from an extended source is imaged as concentric rings (fringes) at the output of the interferometer.

However, restriction of the field of view, imposed by the fiber diameter, created only one fringe as shown earlier in figure 2. The fringe-forming lens, which ultimately images the fiber face on the image dissector, was made of two camera lenses with suitable separation for an effective focal length of 2909 mm. The large magnification ratio of the setup created a 16 mm diameter image of the 0.55 mm diameter fiber on an image dissector. The image dissector was made of two concentric and slightly tilted mirrors. The inner one had a diameter of 10 mm and directed the inner part of the fringe to PMT2, while the 25 mm diameter outer one directed the outer part of the fringe to PMT3. The ratio of light intensities from PMT2 and PMT3 provided a measure of either axial or radial velocity as described earlier.

The success of the velocity measurement system was critically dependent on stable operation of the interferometer. Slight thermal drift or change in the incident laser frequency displaced the reference fringe (fig. 2(a)), which was manifested as an artificial bias in velocity measurement. This made the auto-alignment setup (fig. 4) necessary. The alignment system was a feedback control that first measured the reference fringe diameter and compared it with a prescribed targeted diameter. This was accomplished by splitting parts of the transmitted light using a 3-prism assembly, and imaging them on a CCD camera. Subsequently, the difference between the targeted and the measured fringe diameters was translated into a change of high voltage supply to the piezo-electric actuators that adjusted interferometer's plate separation. Before every Rayleigh measurement, reference light was collected and the auto-alignment system was engaged. When the desired fringe diameter was obtained within a tolerance, the reference light collection system was disengaged, and velocity and density measurement via analysis of Rayleigh scattered light began.

Photoelectron counting electronics were used with all 3 PMT signals. The photoelectron pulses from each PMT arriving within a preset gated time interval was counted using a PC counter-timer board. Counting was performed on contiguous series of gated time intervals without any dead time between the gates. Long time records of up to 5 million data points from each PMT were acquired with a typical sampling rate of 90,000/sec. The data points were converted to physical parameters: instantaneous density and velocity through the usage of proper calibration constants. The Welch method of modified Periodograms (Welch, 1967) was used to calculate individual power spectra and cross-spectra. Each long record was divided into small, 50 percent overlapped, segments; modified periodograms of each segment provided local estimates; average of all local estimates provided the final power spectra. Time domain correlation calculations were also performed via Fourier transform, where individual segments of velocity and density time histories were Fourier transformed, multiplied and inverse transformed. For example, the density-velocity cross-correlation was calculated as:

$$\langle \rho'; u' \rangle = \Im^{-1}\left(\Im(\rho(t)) * \Im^{*}(u(t))\right) \tag{16}$$

In this equation $\Im$ represents Fourier transform, complex conjugation is represented by the superscript *, and inverse Fourier transformation by $\Im^{-1}$. Average of local estimates produced the final correlation. The length of the data segment was varied to assure independency of the calculated values on string length.

III. Results

Validation of the Technique

Figure 5 presents a comparison of the velocity fluctuations spectra measured using the Rayleigh technique and a hot-wire probe. This figure shows that the shapes of velocity spectra are similar while the absolute energy level in the spectrum measured by the Rayleigh technique is two and a half times of that measured by hot-wire. The Rayleigh spectra float on constant white noise floors, which are expected consequences of electronic shot noise. Electronic shot noise creates the unavoidable, fundamental uncertainty in all optical intensity measurements. The photoelectron count in every time bin is

contaminated by random fluctuations that follow Poisson distribution. Spectra calculated from the time series of photoelectron counts obtained from still air, where there is no density or velocity fluctuations, show a white noise floor. The broadband, frequency independent, flat spectrum is a property of electronic shot noise. The propagation of electronic shot noise in the velocity spectrum is somewhat complicated by the ratio of photoelectron counts, $R = N_3/N_2$, needed to determine instantaneous velocity. Nevertheless, the above spectral property was used to extract standard deviation of the velocity fluctuations from the spectra. The measured fluctuations spectra $S_{u'^2}$ is due to a sum of the contributions from the shot noise (with mean square value σ^2_{shot}) and the desired velocity fluctuations (mean-square u'^2_{rms}). The total energy under the power spectrum can be expressed as (Saleh and Teich 1991):

$$\int S_{u'^2}\,df = u'^2_{rms} + \sigma^2_{shot} \tag{17}$$

The constant shot noise floor was estimated as the spectral density value at the highest resolved frequency (Nyquest limit) of 45KHz: $S_{shot} = \left(S_{u'^2}\right)_{f=45000}$ where it was known that the energy from turbulent fluctuations was small. Figure 5 shows the estimated noise floor for each Rayleigh spectra.

$$\text{Since } \sigma^2_{shot} = \int \left(S_{u'^2}\right)_{f=45000} df\ , \tag{18}$$

the standard deviation of velocity fluctuations is:

$$u'_{rms} = \sqrt{\int \left[S_{u'^2} - \left(S_{u'^2}\right)_{f=45000}\right] df}\ . \tag{19}$$

The rms values measured by this shot noise subtraction process are found to be reasonable. For example, in figure 7(a) $(u'_{rms}/U_j)_{hot\text{-}wire} = 0.166$ and $(u'_{rms}/U_j)_{Rayleigh\ corrected} = 0.154$ and in figure 7(b) $(u'_{rms}/U_j)_{hot\text{-}wire} = 0.14$ and $(u'_{rms}/U_j)_{Rayleigh\ corrected} = 0.132$. The subtraction method was used uniformly to estimate ρ'_{rms} and u'_{rms} from respective spectra.

Figures 6(a), 6(b), 7(a), and 7(b) show typical velocity and density fluctuations spectra obtained from a region of very high turbulent fluctuations in Mach 1.4 and 0.95 plumes. Hot-wire is unusable in these jets and spectra measured by Rayleigh technique are shown. It is to be pointed out that the presented velocity and density spectra were narrow-band filter around 430 Hz. The unfiltered velocity data show a large spike at this frequency. The spike was found to be independent of the jet speed and was attributed to a spurious oscillation in the incident laser frequency. As mentioned earlier, the laser head was placed directly underneath the jet and the high noise level created by the plume is suspected to cause small vibration in the laser cavity leading to the spike (Panda et al. 2003). Nonetheless, the density and velocity fluctuations spectra are similar in shape. For data in figures 6 and 7 the spectra show significant energy in the lowest frequency. The high frequency roll-off is masked by the shot noise floor.

The cross-correlation calculations between density and velocity fluctuations, however; are mostly unaffected by shot noise. Since the shot noise from different PMT are uncorrelated, the cross-correlation process eliminates the influence of electronic shot noise and the absolute cross-correlation values are expected to have very small uncertainty. Parts (c) and (d) of figures 6 and 7 presents the non-dimensionalized cross-correlation values measured in two different Mach number jets. Note that the correlations are expected to be symmetric in time; only the positive time delays are shown here. There are multiple interesting observations that can be made from these figures. First, $<\rho';u'>$ correlations are always fairly high and mostly positive. Second, $<\rho';u'u'>$ correlations can be high or low depending on the Mach number and probe locations. In the present unheated jets positive values of the $<\rho';u'>$ correlation are expected. The unheated jets cool to lower temperatures and higher densities than the ambient upon

expansion through the nozzle. Since the high velocity is associated with the high density (jet air) and the low velocity with the low density (entrained ambient air) $<\rho';u'>$ correlations are positive. It is expected that if the same experiments were conducted in a heated jet, with core density lower than the ambient, negative correlations would have resulted. The $<\rho';u'u'>$ correlations, on the other hand; do not follow this argument. Following is a discussion of the uncertainty in the cross-correlation data.

The correlation values are normalized by individual standard deviations which are the primary sources of uncertainty in the presented form. For example, correlations between velocity and density fluctuations are expressed as $\dfrac{\langle \rho';u' \rangle}{\rho'_{rms}\, u'_{rms}}$, which requires estimates of u'_{rms} and ρ'_{rms}. As mentioned above $<\rho';u'>$ correlations are relatively error free, however; the shot noise subtraction process described earlier has to be used to determine u'_{rms} and ρ'_{rms}. The subtraction process creates ±10 percent error in the standard deviation estimates. Hence, uncertainty levels of ±20 percent are expected on the quoted normalized correlation values. This large uncertainty supersedes all other sources, such as the contamination from temperature fluctuations, numerical convergence error etc.

The differences between Favre averaged and Reynolds averaged values are straightforward to calculate from the measured correlation data. For example, for the conditions shown in figure 7 the normalized differences between the Favre-averaged and time-averaged axial velocity is calculated from equations (5) and (12), using additional measured values of $\bar{\rho}$ = 1.44 Kg/m^3, $\bar{u}$ = 391m/s and $\overline{u'^2}$ = 1028 (m/s)^2:

$$\frac{\tilde{u}-\bar{u}}{\bar{u}} = \frac{\langle \rho';u' \rangle_{\tau=0}}{\bar{\rho}\,\bar{u}} = 0.004.$$

Note that the large uncertainty in the normalized $<\rho';u'>/(\rho'_{rms}\, u'_{rms})$ does not affect the above estimate. Since the absolute values of the correlations are measured relatively accurately, the primary source of error is the uncertainty in $\bar{\rho}$ and $\bar{u}$ measurement. It is estimated that $(\tilde{u}-\bar{u})/\bar{u}$ is determinable within a maximum of ±10 percent uncertainty. The difference in the kinetic energy associated with the axial velocity fluctuations is calculated using equations (10) and (12):

$$\frac{\widetilde{u''u''}-\overline{u'u'}}{\overline{u'u'}} = \frac{1}{\overline{u'^2}}\left(\frac{\langle \rho';u'u' \rangle_{\tau=0}}{\bar{\rho}} - \left(\frac{\langle \rho';u' \rangle_{\tau=0}}{\bar{\rho}} \right)^2 \right)$$
$$= -0.038$$

The uncertainty in the above calculation is relatively higher due to the uncertainty in the $\overline{u'^2}$ estimates. The estimated level is ±25 percent of the quoted number.

A large number of data points were measured from many axial and radial locations in different Mach number plumes. Data analyzed from some selected conditions are shown in table I. A closer look into this table confirms previous observations on $<\rho';u'>$ and $<\rho';u'u'>$ correlations. Additionally it confirms that the Favre averaged velocity is very slightly (fraction of a percent to one percent) higher than the Reynolds averaged counterpart. Favre-averaging also produces lower level (fraction of a percent to four percent) of kinetic energy compared to the Reynolds averaging. Notably $<\rho';u'u'>$ correlations have stronger impact than $<\rho';u'>$ correlations on the differences in the kinetic energy; a larger value of the former reflects as a larger differences between the two averaging process.

Table I also provides a comparison of the measured air density fluctuations $\rho'_{rms}/\bar{\rho}$ with that estimated from velocity fluctuations $u'_{rms}/\bar{u}$ using Morkovin's hypothesis (eq. (3)). Morkovin's hypothesis is always found to under-predict fluctuations at all Mach number conditions. The differences are particularly large in regions with vigorous turbulent fluctuations such as the end of the potential core and the middle of the lip shear layer.

IV. Summary and Conclusion

A molecular Rayleigh scattering based optical measurement technique was used to simultaneously measure air density and the axial component of velocity at a sampling rate of 90,000/sec. The density variation was measured by monitoring the variation of the total scattered light intensity. The velocity variation was measured by spectrally resolving the scattered light using a Fabry-Perot interferometer and monitoring the time dependent Doppler shift from the incident laser frequency. A small probe volume length of 1.06 mm and diameter 0.2 mm^2 allowed point measurement from different regions of the flow-field. One convergent and two convergent-divergent nozzles were used to produce unheated plumes in Mach numbers 0.8, 0.95, 1.4 and 1.8. The standard deviations of the density ρ'_{rms} and axial velocity u'_{rms} fluctuations and the density-velocity $<\rho';u'>$ and density-velocity^2 $<\rho';u'u'>$ cross-correlations measured from different regions of the plumes provided the following results.

(a) Normalized $\overline{\rho' u'}$ correlations are significantly high (varies between 0.2 and 0.7) and almost always positive. The positive correlation is expected in the unheated plume where the jet core has higher density than the ambient.

(b) Normalized $\overline{\rho' u' u'}$ correlations are also high (mostly varies between –0.1 and –0.5) and always negative.

(c) The Favre averaged axial velocity is very slightly (fraction of a percent to one percent) higher than the Reynolds averaged counterpart.

(d) The axial component of turbulent kinetic energy calculated via Favre-averaging, $0.5\,\widetilde{u''u''}$, is lower by a fraction of a percent to four percent from the same calculated via Reynolds averaging $0.5\overline{u'u'}$.

(e) Estimation of turbulent density fluctuations, from the axial velocity fluctuations using Morkovin's hypothesis, is found to provide lower values compared to the measured data at all Mach number conditions.

The present experiments were conducted in unheated jets where the stagnation temperature of the plume was the same as that of the ambient. It will be of interest to conduct similar experiments in heated jets where the effect of total temperature fluctuations on the above parameters can be established.

References

Bowersox, R.D.W. 1996 Combined Laser Doppler Velocimetry and Cross-Wire Anemometry Analysis for Supersonic Turbulent Flow, *AIAA J.,* **34** (11), 2269-2275.

Favre, A. 1976 Équations fondamentales des fluids à masse volumique variable en écoulements turbulents. Pages 24–78 of: Favre, A., Kovasznay, L.S.G., Dumas, R., Gaviglio, J., and Coantic, M. (eds.), *La Turbulence en Mécanique des Fluides*; CNRS.

Lele, S.K., 1994 Compressibility effects on Turbulence, *Ann Rev. Fl. Mech.,* **26**, 211–254.

Panda, J. and Seasholtz, R.G. 2002 Experimental Investigation of density fluctuations in high-speed jets and correlation with generated noise. *J. Fluid Mech.,* **450**, 97–130.

Panda, J., Seasholtz, R.G., Elam, K.A., and Mielke, A.F. 2004 Time-averaged velocity, temperature and density surveys of supersonic free jets, *ASME paper number HT-FED2004-56856*.

Panda, J., Seasholtz, R.G., and Elam, K.A. 2003 "Further Progress in Noise Source Identification in High Speed Jets Via Causality Principle", AIAA paper 2003-3126, also submitted to *Journal of Fluid Mechanics.*

Saleh, B.E.A. and Teich, M.C. 1991 *Fundamentals of Photonics*, John Wiley & Sons, New York.

Seasholtz, R.G., Panda, J., and Elam, K.A. 2001 Rayleigh Scattering Diagnostics for Dynamic Measurement of Velocity Fluctuations in High Speed Jets. *AIAA paper no 2001-0847.*

Seasholtz, R.G., Panda, J., and Elam, K.A. 2002 Rayleigh Scattering Diagnostic for Measurement of Velocity and Density Fluctuation Spectra. 40th AIAA Aerospace Sciences meeting, *AIAA paper no 2002–0827.*

Bradshaw, P. 1977 Compressible Turbulent Shear Layers, Ann. Rev. Fluid Mech., **9**, 33–54.

TABLE I.—STANDARD DEVIATIONS OF DENSITY AND VELOCITY FLUCTUATIONS, CORRELATIONS BETWEEN THE TWO, AND THEIR IMPACT ON FAVRE AVERAGING AND STRONG REYNOLDS ANALOGY.

Mj	x/D	r/D	File name	$\frac{u'_{rms}}{\bar{u}}$	$\frac{\rho'_{rms}}{\bar{\rho}}$	$\left(\frac{\rho'_{rms}}{\bar{\rho}}\right)_{predict} = (\gamma-1)M^2\frac{u'_{rms}}{\bar{u}}$	$\frac{\langle \rho'; u' \rangle_{\tau=0}}{\rho'_{rms} u'_{rms}}$	$\frac{\langle \rho'; u'u' \rangle_{\tau=0}}{\rho'_{rms} (u'u')_{rms}}$	$\frac{\tilde{U}-\bar{U}}{\bar{U}}$	$\frac{\widetilde{u''u''} - \overline{u'u'}}{\overline{u'u'}}$
1.8	6	0	Oct30-1113	0.042	0.041	0.031	–0.3213	–0.067	–0.0006	–0.003
	8	0	Oct30–1114	0.048	0.05	0.042	–0.34	–0.123	–0.0008	–0.006
	10	0	Oct30–1115	0.064	0.07	0.049	0.24	–0.384	0.001	–0.028
	12	0	Oct30–1116	0.096	0.096	0.064	0.56	–0.402	0.005	–0.04
	14	0	Oct30–1117	0.127	0.093	0.072	0.618	–0.215	0.007	–0.023
	16	0	Oct30–1118	0.15	0.093	0.069	0.59	–0.052	0.008	–0.008
	3	0.45	Oct30–1134	0.046	0.051	0.036	0.14	–0.26	0.0003	–0.013
	4	0.45	Oct30–1133	0.068	0.072	0.05	0.65	–0.55	0.003	–0.042
	6*	0.45	Oct30–1130	0.11	0.09	0.064	0.72	–0.35	0.008	–0.038
	8	0.45	Oct30–1129	0.134	0.10	0.067	0.705	–0.205	0.009	–0.026
	10	0.45	Oct30–1126	0.15	0.10	0.07	0.663	–0.1	0.01	–0.015
	12	0.45	Oct30–1125	0.17	0.1	0.068	0.635	–0.045	0.011	–0.009
1.4	10	0	Jul25–1104	0.08	0.079	0.042	0.59	–0.39	0.004	–0.038
	10	0.2	Jan31–1073	0.112	0.086	0.045	0.56	–0.12	0.005	–0.013
	10	0.4	Jan31–1075	0.2	0.08	0.056	0.49	–0.22	0.008	–0.02
	10	0.6	Jan31–1077	0.27	0.067	0.044	0.38	–0.005	0.007	–0.001
	10	0.8	Jan31–1078	0.32	0.06	0.027	0.223	0.16	0.005	0.01
	4	0.45	Jul25–1073	0.16	0.05	0.03	0.38	–0.15	0.003	–0.008
	14	0	Jul25–1069	0.17	0.04	0.03	0.2	–0.48	0.002	–0.002
0.95	10	0	Jul25–1062	0.11	0.055	0.026	0.36	–0.13	0.002	–0.007
	14	0	Jul25–1068	0.12	0.04	0.02	0.2	0.03	0.001	0.001
	4	0.45	Jul25–1073	0.16	0.05	0.03	0.38	–0.15	0.003	–0.008
	6	0.45	Jul25–1076	0.2	0.05	0.03	0.35	–0.2	0.003	–0.01
	10	0.45	Jul25–1080	0.24	0.05	0.03	0.29	–0.13	0.003	–0.007
0.8	8	0	Jul25–1084	0.08	0.04	0.02	0.22	–0.1	0.0008	–0.005

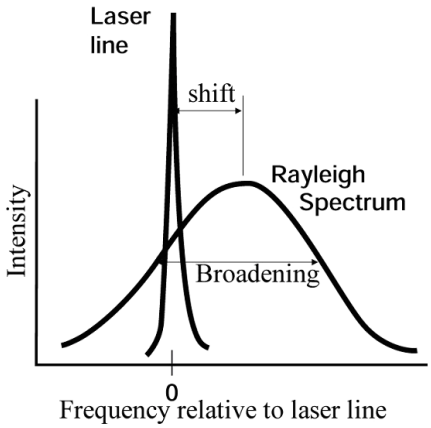

Figure 1.—Schematic of Rayleigh spectrum from air flow.

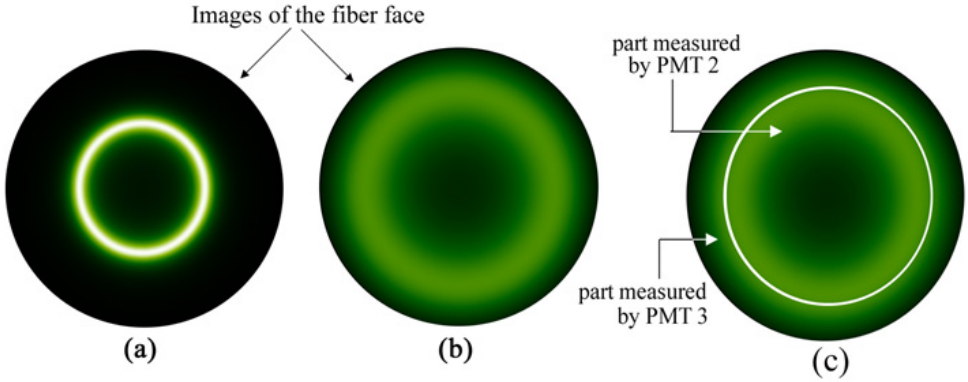

Figure 2.—Fringes formed after passing through Fabry–Perot Interferometer by (a) incident laser light (b) Rayleigh scattered light; (c) splitting of Rayleigh image to measure velocity fluctuations.

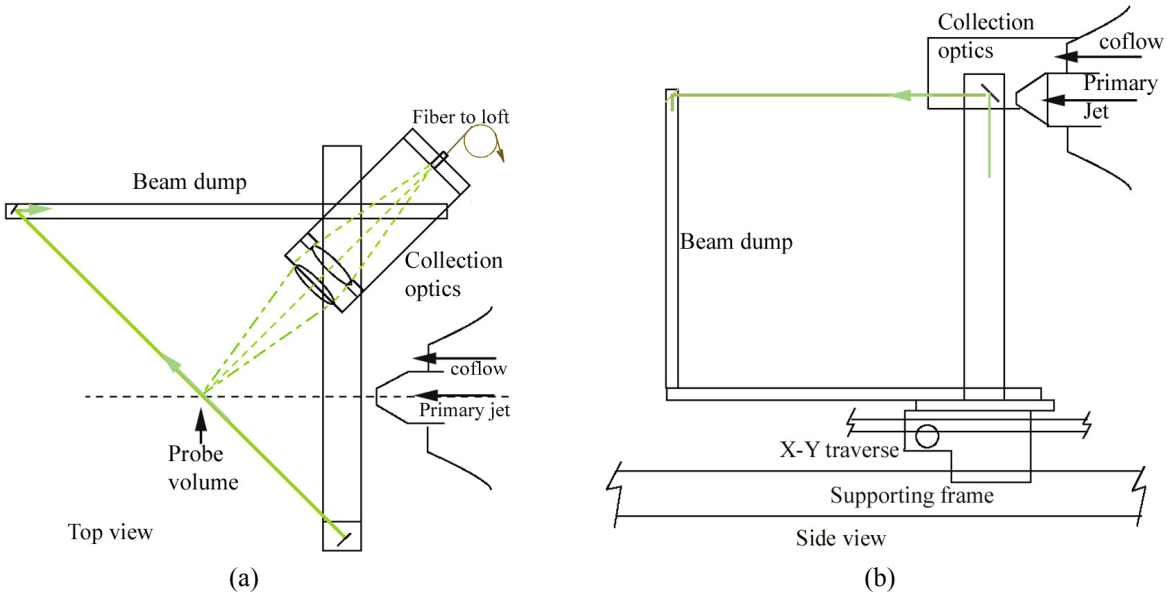

Figure 3.—(a) Top view of optical arrangement to measure axial u component of velocity. (b) Side view.

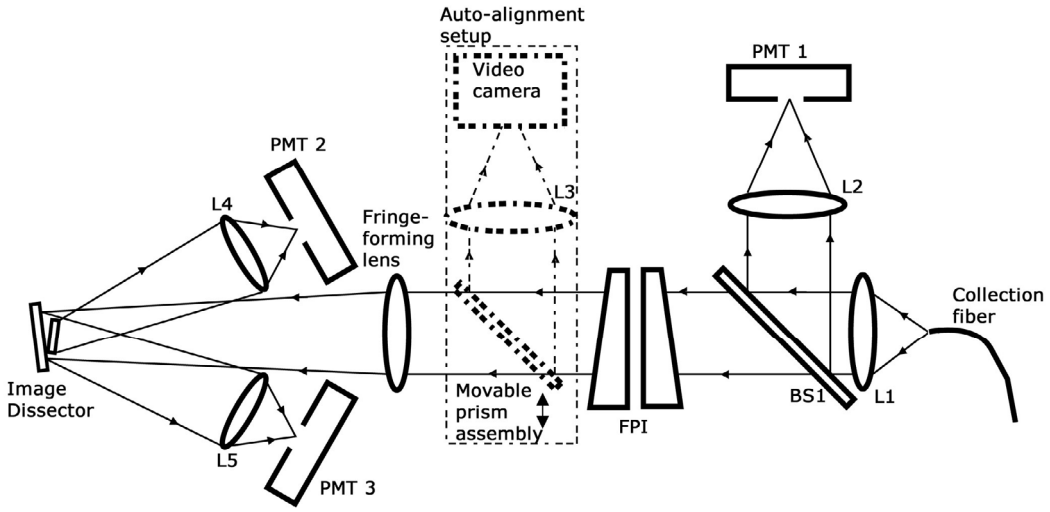

Figure 4.—Schematic of optical setup to analyze collected light. L1 to L5 are lenses; BS1 is beam–splitter and FPI is the Fabry–Perot interferometer.

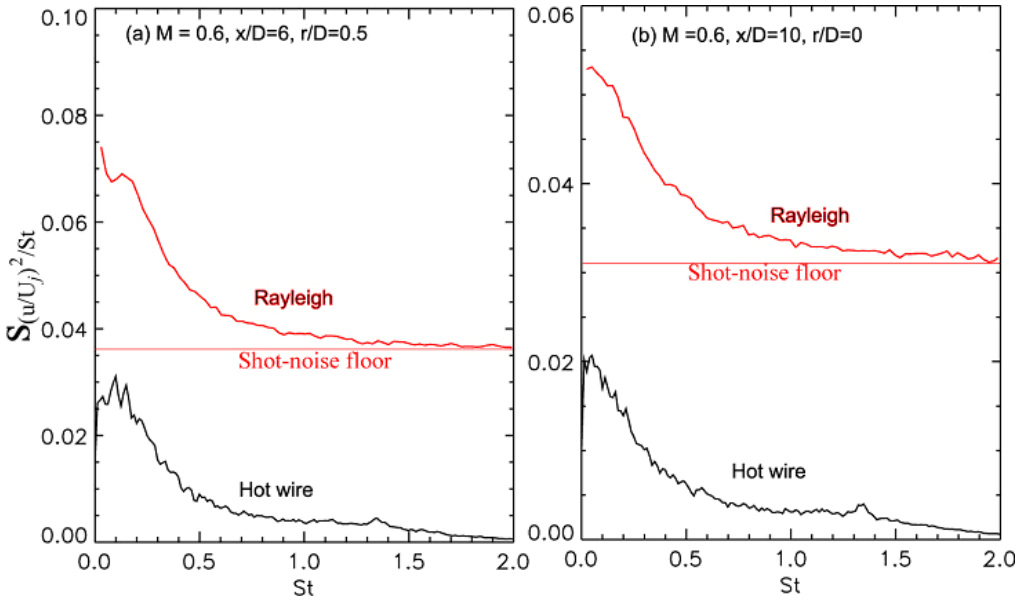

Figure 5.—A comparison of power spectral density of u fluctuations measured by the Rayleigh technique and a hot–wire probe at indicated locations of Mach 0.6 plume.

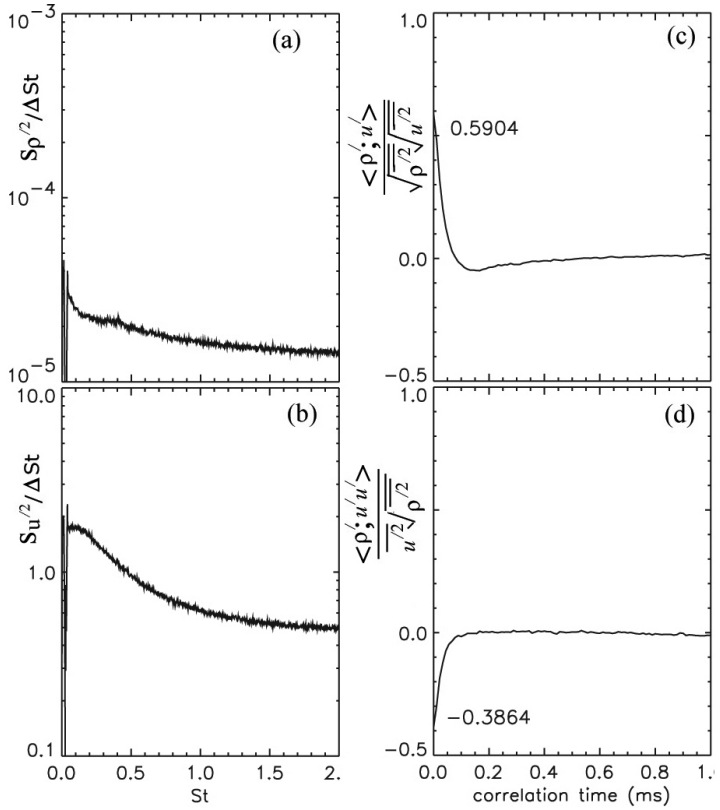

Figure 6.—Power spectral density of (a) air density fluctuations and (b) axial velocity fluctuations. Correlation between (c) density–velocity fluctuations, and (d) density–velocity^2 fluctuations measured at x/D =10, r/D=0 in a Mach 1.4 jet.

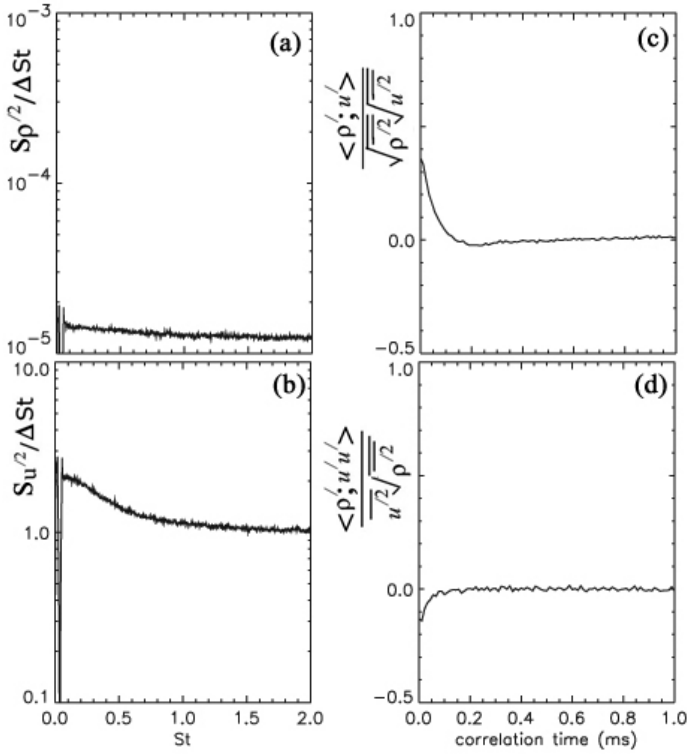

Figure 7.—Same as figure 6 except M=0.95 jet, probe volume location x/D=10 and centerline.

REPORT DOCUMENTATION PAGE

Form Approved
OMB No. 0704-0188

1. AGENCY USE ONLY (*Leave blank*)	2. REPORT DATE	3. REPORT TYPE AND DATES COVERED
	May 2005	Technical Memorandum

4. TITLE AND SUBTITLE

Experimental Investigation of the Differences Between Reynolds-Averaged and Favre-Averaged Velocity in Supersonic Jets

5. FUNDING NUMBERS

WBS–22–781–30–61

6. AUTHOR(S)

J. Panda and R.G. Seasholtz

7. PERFORMING ORGANIZATION NAME(S) AND ADDRESS(ES)

National Aeronautics and Space Administration
John H. Glenn Research Center at Lewis Field
Cleveland, Ohio 44135–3191

8. PERFORMING ORGANIZATION REPORT NUMBER

E–15009

9. SPONSORING/MONITORING AGENCY NAME(S) AND ADDRESS(ES)

National Aeronautics and Space Administration
Washington, DC 20546–0001

10. SPONSORING/MONITORING AGENCY REPORT NUMBER

NASA TM—2005-213564
AIAA–2005–0514

11. SUPPLEMENTARY NOTES

Prepared for the 43rd Aerospace Sciences Meeting and Exhibit sponsored by the American Institute of Aeronautics and Astronautics, Reno, Nevada, January 10–13, 2005. J. Panda, Ohio Aerospace Institute, 22800 Cedar Point Road, Brook Park, Ohio 44142; and R.G. Seasholtz, NASA Glenn Research Center. Responsible person, R.G. Seasholtz, organization code RIO, 216–433–3754.

12a. DISTRIBUTION/AVAILABILITY STATEMENT

Unclassified - Unlimited
Subject Category: 36

Available electronically at http://gltrs.grc.nasa.gov

This publication is available from the NASA Center for AeroSpace Information, 301–621–0390.

12b. DISTRIBUTION CODE

13. ABSTRACT ***(Maximum 200 words)***

Recent advancement in the molecular Rayleigh scattering based technique allowed for simultaneous measurement of velocity and density fluctuations with high sampling rates. The technique was used to investigate unheated high subsonic and supersonic fully expanded free jets in the Mach number range of 0.8 to 1.8. The difference between the Favre averaged and Reynolds averaged axial velocity and axial component of the turbulent kinetic energy is found to be small. Estimates based on the Morkovin's 'Strong Reynolds Analogy' were found to provide lower values of turbulent density fluctuations than the measured data.

14. SUBJECT TERMS

Nozzle flow; Flow velocity; Rayleigh scattering

15. NUMBER OF PAGES

22

16. PRICE CODE

17. SECURITY CLASSIFICATION OF REPORT	18. SECURITY CLASSIFICATION OF THIS PAGE	19. SECURITY CLASSIFICATION OF ABSTRACT	20. LIMITATION OF ABSTRACT
Unclassified	Unclassified	Unclassified	